# 30-kW Performance of a 100-kW Class Nested-channel Hall Thruster

**IEPC-2015-125/ISTS-2015-b-125**

*Presented at Joint Conference of 30th International Symposium on Space Technology and Science,*
*34th International Electric Propulsion Conference and 6th Nano-satellite Symposium*
*Hyogo-Kobe, Japan*
*July 4–10, 2015*

Scott J. Hall,* Sarah E. Cusson,† and Alec D. Gallimore‡
*University of Michigan, Ann Arbor, Michigan, 48109, USA*

**Performance up to 30 kW discharge power of a 100-kW class, 3-channel nested Hall thruster operating on xenon propellant is presented. Each of the seven combinations of thruster channels were run at 75% of the nominal thruster current density and 300 V anode potential. Discharge power ranged from 4 kW for the inner channel on its own to 30 kW for all three channels operating together. Thrust was measured using a new inverted-pendulum, null-type thrust stand designed to safely support over 250 kg of thruster mass while accurately resolving thrust. With all 3 channels running at 30 kW total discharge power, the anode specific impulse was 1840 s, anode efficiency was 45.0%, and thrust was 1518 mN. Anode specific impulse ranged from 1200 s to 2300 s across operating conditions and anode efficiency ranged from 21% to 67%. A discussion of the effect of chamber backpressure on performance measurements is included. Comparison of X3 performance is made to other state-of-the-art Hall thrusters operating at similar fractions of current density.**

*Ph.D Candidate, Department of Aerospace Engineering, sjhall@umich.edu
†Ph.D Pre-Candidate, Department of Aerospace Engineering, cusson@umich.edu
‡Arthur F. Thurnau Professor of Aerospace Engineering, alec.gallimore@umich.edu

## Nomenclature

$a$ = slope of linear fit
$b$ = intercept of linear fit
$g$ = acceleration due to gravity
$I_D$ = discharge current
$I_{RMS}$ = root mean square discharge current amplitude
$I_{sp,a}$ = anode specific impulse
$j_{nom}$ = nominal current density
$\dot{m}_a$ = anode mass flow rate
$\dot{m}_c$ = total cathode flow rate
$P_D$ = discharge power
$p_b$ = chamber backpressure
$T$ = thrust
$V_{c-g}$ = cathode-to-ground voltage
$V_D$ = discharge voltage
$\Delta T$ = uncertainty of thrust
$\eta_a$ = anode efficiency
$()_I$ = inner channel
$()_{Lower}$ = lower bound of uncertainty
$()_M$ = middle channel
$()_O$ = outer channel
$()_T$ = thruster total (sum of all operating channels)
$()_{Upper}$ = upper bound of uncertainty

# I. Introduction and Motivation

Nested-channel Hall thrusters have been identified as a means to increase Hall thruster power levels above 100 kW while maintaining acceptable device size and mass.[1] In a recent Broad Agency Announcement, NASA identified high-power electric propulsion (up to 300 kW) as enabling for a variety of mission structures, including human space exploration.[2] Additionally, a 2010 NASA team found that high-power electric propulsion was key to allowing affordable travel to asteroids and near-Earth destinations by reducing launch mass up to 50%.[3] NASA hopes to implement a system that has a broad power and specific impulse range for maximum flexibility within a mission. The multiple discharge channels of a nested-channel Hall thruster allows for throttling far beyond that of a single-channel Hall thruster. This essential feature makes these devices ideal candidates for a system to meet NASA's needs and goals.

Following the success of the proof-of-concept X2, a 10-kW class two-channel nested Hall thruster,[4,5] the Plasmadynamics and Electric Propulsion Laboratory (PEPL) at the University of Michigan, in collaboration with NASA and the Air Force Office of Scientific Research, developed the X3, a 100-kW class three-channel nested Hall thruster.[6–8] The thruster, seen in Fig. 1, features the largest throttling capability of any Hall thruster to date, with seven different firing configurations[a] and power levels ranging from 2 kW to 200 kW. This exceptionally wide operating range allows the thruster to achieve both high specific impulse and high thrust operation. Previous work done by Hall[8] validated operation of the thruster up to discharge powers of 61 kW and current densities of 150% nominal. This validation showed proper thruster operation and behavior, and indicated that there was interaction between channels during multi-channel operation.

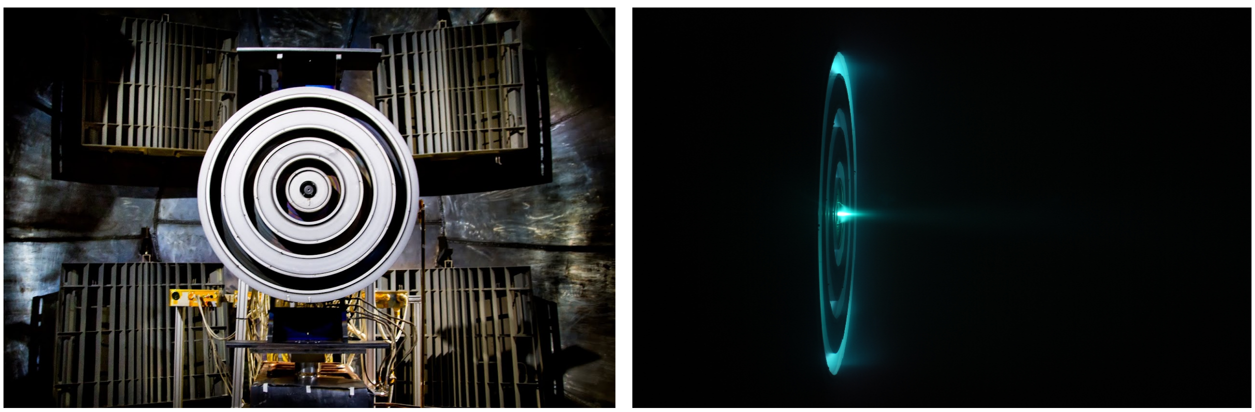

**Figure 1. The X3 100-kW class nested Hall thruster mounted for operation inside the Large Vacuum Test Facility at the University of Michigan (left) and firing in three-channel configuration at 30 kW (right).**

To investigate the performance of the X3 in a low-discharge-current configuration, thrust was measured for every operating configuration of the thruster at 75% nominal current density ($0.75 j_{nom}$) and 300 V anode potential. The work presented here first details the performance of the X3 at the specified operating condition, and then compares this performance to that of other state-of-the-art Hall thrusters at similar current densities and discharge voltages. Section II presents the experimental apparatus, including details of the thruster, cathode, vacuum facility, thrust stand, and test matrix. Section III presents the results and discussion, including performance data, comments on the effects of facility backpressure, a comparison to the performance of the X3 to other state-of-the-art Hall thrusters, and a discussion of the uncertainty analysis undertaken for these data. Finally, conclusions and future work are presented.

# II. Experimental Apparatus

## A. Thruster

The X3 features three discharge channels with similar cross sections, magnetic fields, and gas distributors. The magnetic fields on the inner and outer channel point in the opposite radial direction as the middle channel. During operation, each channel of the thruster went through a ceramic bakeout of 1.5 hours at half the test current density before any experimental data were obtained. Due to the large thermal mass

[a]Each channel can be operated alone or in combination with any or all other channels.

of the thruster, no attempt was made to reach full thermal equilibrium before performance measurements were taken (a similar concession was made with the NASA-457Mv1[9]). Instead, the thruster was typically operated for 30 minutes before data collection, at which point the thruster discharge current was steady and had stopped drifting.

The X3 was run from three separate laboratory power supplies: a 60-kW supply for the inner channel, a 100-kW supply for the middle channel, and a 150-kW supply for the outer channel. Each supply was connected to two 160-$\mu$F capacitors in series to filter the plasma oscillations from the discharge power supplies. The common for all discharge channels was shared through the single centrally-mounted cathode. This configuration is based on what was done with the X2[4] and with thruster clusters sharing a single cathode.[10] During operation, the thruster body was grounded to the facility through the thrust stand.

Power to the six electromagnets and the cathode was supplied using commercially-available rack-mounted power supplies. High-purity xenon propellant was provided to the thruster through five commercially-available mass flow controllers plumbed to stainless steel lines: A 400-sccm controller for the inner channel, an 800-sccm controller for the middle channel, a 3000-sccm controller for the outer channel, a 50-sccm controller for the center cathode flow, and a 1000-sccm controller for the cathode external gas injectors. The mass flow controllers featured uncertainties of $\pm 1\%$ of their maximum flow rate. Flow controllers were all calibrated before operation with a volumetric flow calibrator with an accuracy of 1%. Multiple points were taken for each controller and a linear fit was used to calculate the controller set point for any arbitrary flow rate.

Discharge current oscillations were non-invasively monitored using three commercially-available current sensors each attached to a commercially-available amplifier. AC-coupled discharge current was measured with precision down to 5 mA.

## B. Cathode

The X3 operates with a single centrally-mounted cathode. Both NASA Glenn Research Center and the Jet Propulsion Laboratory, California Institute of Technology (JPL), built cathodes for X3 operation. For this test, as for all X3 operation to date, the JPL cathode was used. This cathode, described previously,[11] is a 275-A lanthanum-hexaboride hollow cathode that features external gas injectors to help reduce cathode erosion.[12] The cathode was operated at a constant 10% flow fraction of the total flow rate through all anodes. Up to 2 mg/s flowed through the central cathode body, and the remainder of the 10% flowed through the external injectors.

## C. Vacuum Facility

These experiments were performed in the Large Vacuum Test Facility (LVTF) at the University of Michigan. The LVTF is a 9-meter long, 6-meter diameter stainless-steel clad vacuum chamber that was brought to rough vacuum (100-mTorr range) using four 400-CFM mechanical pumps and two 2000-CFM blowers. Base pressures of about $3\times10^{-7}$ Torr were achieved with seven TM1200 re-entrant cryopumps with liquid-nitrogen-cooled shrouds. The cryopump system featured a nominal pumping speed of 500,000 liters per second on air and 240,000 liters per second on xenon.

Pressure was measured in the LVTF using an internally-mounted Varian 571 Bayard-Alpert style ionization gauge. The gauge featured a grid on the entrance that was electrically floating. The uncertainty on the gauge is reported by the manufacturer as $\pm 20\%$. The gauge was mounted approximately on thruster exit plane at the bottom of the thrust stand, as shown in Fig. 2. As described in the best

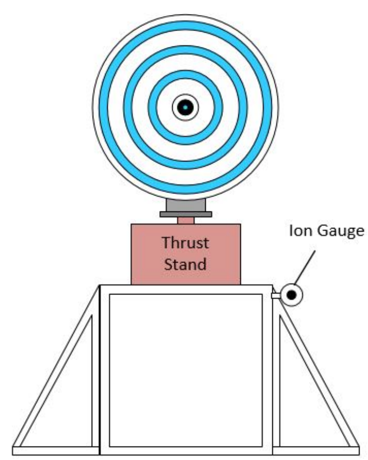


**Figure 2. Schematic of ion gauge location relative to thruster.**

practices for pressure measurement by Dankovich,[13] the entrance of the gauge was positioned in the same orientation as the thruster exit plane (i.e., facing the beam dump).

### D. Thrust Stand

A new thrust stand was necessary to properly resolve thrust while safely supporting the mass of the X3. To simplify implementation, the stand was designed such that it shared many qualities with PEPL's previous inverted-pendulum thrust stand (which is functionally similar to what was described by Xu and Walker[14]). The new stand was an inverted pendulum design that featured a linear variable differential transformer (LVDT) to measure displacement. The LVDT signal was fed to a commercially-available PID controller that used an electromagnetic coil to maintain the thrust stand in its "null" position. The response of this coil was used to calculate thrust using a calibration of known weights before and after thruster firing. The drift in the PID signal zero during thruster operation was accounted for through calibrations and data post-processing. Error reduction practices as described by Polk[15] were employed.

The traditional shim-stock flexure design as described in Xu and Walker was rejected due to concerns about the mass of the X3 (which is greater than 250 kg). In its place, a much more robust design was implemented based on designs used at the Air Force Research Laboratory. This design used torsional bearings as opposed to shim-stock flexures to provide better support against buckling. The torsional bearings provided a spring-like resistive force to oppose thrust; additional resistance to thrust was provided by stainless steel tensile springs. A schematic of this design is provided in Fig. 3.

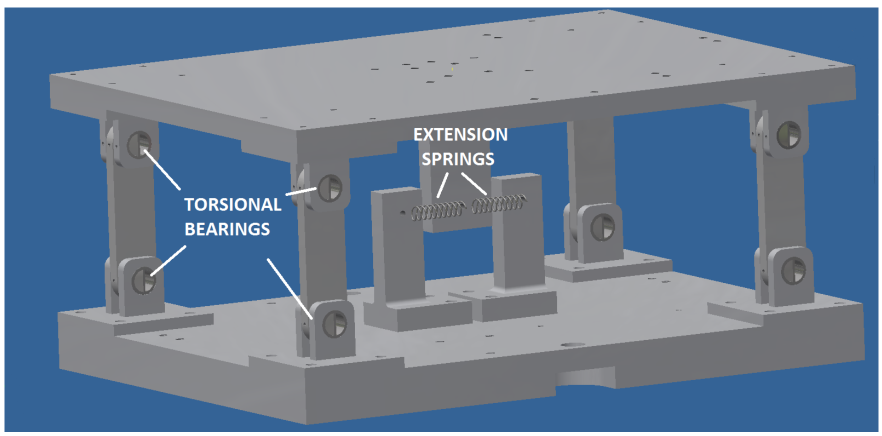


**Figure 3. A computer model of the support and spring system used in the X3 thrust stand, with the torsional bearings and extension springs highlighted.**

The thrust stand was leveled using a fine-thread screw attached to an electric motor that was controlled manually from outside the vacuum chamber to tip the stand. Drift in the inclination was seen during thruster operation, which was corrected in-situ using the motor and screw. Due to the weight of the X3, the stand was found to be extremely sensitive to leveling, up to the precision the motor and screw were able to provide. This contributed some to the large uncertainty seen in some of the measurements. A more detailed discussion of uncertainty analysis is provided in Section III-E.

### E. Test Matrix

The X3 was operated previously at two current densities inside the LVTF during its initial characterization:[8] $0.75 j_{nom}$ and $1.5 j_{nom}$. During that test, there was no concern for chamber backpressure. However, the backpressure limit for Hall thruster performance testing has been established at 30 $\mu$Torr-Xe.[13] In an attempt to limit the backpressure of these experiments to as close to this established limit as possible within the LVTF, only the lower current density was tested. At this current density, there was interest in increasing the discharge voltage above 300 V. However, during this process, non-thruster electrical infrastructure issues led to the test ending prematurely.

As such, only the 300 V/$0.75 j_{nom}$ operation is reported here. At these settings, each channel was operated at constant power; that is, discharge current for each channel was held constant, controlled by anode mass flow rate. This constant-power operation was chosen over constant-mass-flow-rate operation because it better accounted for the variation in backpressure across different thruster operational modes. By maintaining power, thrust should theoretically be the same regardless of backpressure. Work by Hofer[16] showed that this was not strictly the case for the H6MS (a single-channel, magnetically-shielded thruster), but that a centrally-mounted cathode reduced the backpressure sensitivity to negligible levels as compared to an externally mounted one. Though anode efficiency and anode specific impulse will be lower at lower backpressure (because the flow rates needed to maintain discharge power are higher, as the thruster is ingesting less background gas), the lower values are more indicative of expected "in-space" values than those found by artificially raising chamber backpressure to match across all operating conditions.

A summary of the test conditions for these experiments is presented in Table 1. It should be noted that the thruster was operated at "optimized" magnetic field settings at each operating point based on previous work completed by Florenz,[17] instead of a single magnetic field across all conditions. The changes across conditions were typically minor in both strength and shape, but are significant enough to be noted. Though a common magnetic field would help determine any performance boost from multiple-channel interaction, for an experiment focused simply on thruster performance such as this, optimizing the field for each condition was seen as more agreeable with the experiment's goals.

**Table 1. The throttling table for this experiment. Note that all operation was performed at 300 V anode potential.**

| Condition | $I_{D,I}$ | $I_{D,M}$ | $I_{D,O}$ | $I_{D,T}$ | $P_{D,T}$ |
|---|---|---|---|---|---|
| I | 13.5 A | – | – | 13.5 A | 4.1 kW |
| M | – | 31.5 A | – | 31.5 A | 9.5 kW |
| O | – | – | 54.8 A | 54.8 A | 16.4 kW |
| I+M | 13.5 A | 31.5 A | – | 45 A | 13.6 kW |
| I+O | 13.5 A | – | 54.8 A | 68.3 A | 20.5 kW |
| M+O | – | 31.5 A | 54.8 A | 86.3 A | 25.9 kW |
| I+M+O | 13.5 A | 31.5 A | 54.8 A | 100 A | 30 kW |

# III. Results and Discussion

## A. Performance

Three performance metrics were analyzed in this experiment. First was thrust, which was directly measured. This value was combined with the measured thruster telemetry (specifically discharge current, discharge voltage, and mass flow rates) to calculate both anode efficiency:

$$\eta_a = \frac{T^2}{2 \cdot \dot{m}_a \cdot P_d} \tag{1}$$

and anode specific impulse:

$$I_{sp,a} = \frac{T}{\dot{m}_a \cdot g} \tag{2}$$

where $T$ is the measured thrust value, $\dot{m}_a$ is anode mass flow rate, $P_d$ is discharge power, and $g$ is the acceleration due to Earth's gravity. The anode quantities are studied here because no effort was made to optimize cathode performance or to minimize electromagnet power.

Thrust versus discharge power is presented in Fig. 4. It can be seen that the thrust increases as discharge power increases, which is to be expected. Multiple-channel conditions appear to fall along a thrust/power line with a steeper slope than the single-channel conditions. The data clearly indicate that there is a boost in thrust for a given input power with the I+M condition, which has higher thrust but lower input power than the O condition. If this trend continues to hold true across future X3 operation, it would indicate a performance boost from multi-channel operation.

Figure 5 shows anode specific impulse versus discharge power. This plot indicates that for all multi-channel operating conditions, the anode specific impulse is at least equal to that of the highest relevant single-channel case. The I+M condition sees a boost in specific impulse over the inner channel alone, though

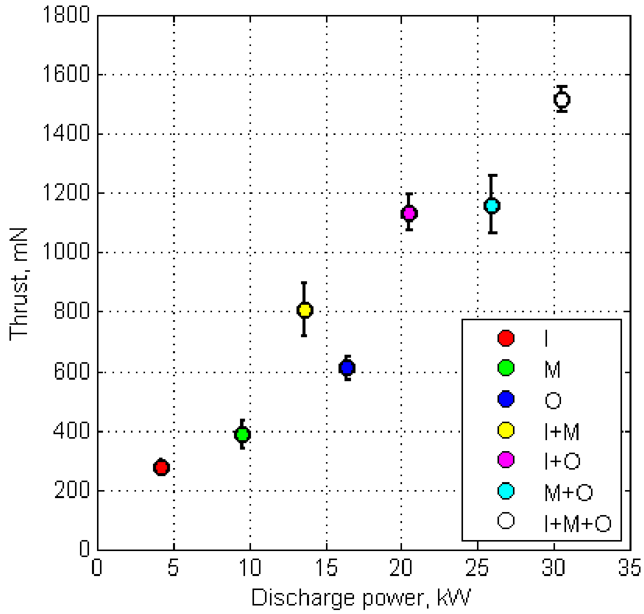


**Figure 4. Thrust versus power across all operating conditions.**

for that condition the uncertainty is large enough that the boost is barely statistically significant. The uncertainty in both anode specific impulse and anode efficiency predominantly come from the uncertainty in the thrust measurement. More detail on uncertainty analysis of thrust values is given in Section III-E.

Anode efficiency versus discharge power is shown in Fig. 6. Here, the trend is less clear. The I+M condition provides an efficiency higher than that of the inner or middle alone (and in fact the highest efficiency of the entire set); M+O also provides a slightly higher efficiency than either channel separately; the remaining multi-channel cases (I+O and I+M+O) have efficiencies that fall between the values of the channels operating alone. The reason for this is unclear. Again, the large uncertainty on two of the conditions obscures any trends.

One final metric of thruster performance, thrust-to-power ratio (T/P), is plotted in Fig. 7. This shows that the I condition was operating at a particularly high T/P, whereas the M, O, and M+O conditions are at both low anode specific impulses and low T/P. The multi-channel conditions all fall at T/Ps above the M and O conditions but below the I condition, showing "averaging" behavior similar to what was seen in the anode specific impulse and anode efficiency of some multi-channel conditions.

The efficiencies, specific impulses, and T/P of the M, O, and M+O conditions are unexpectedly low. Reasons for this are unclear, and further experiments are necessary. Suspected mechanisms include possible cathode coupling issues: the middle channel's magnetic lens is separated from the cathode by one magnetic lens topology, and the outer channel's by two. As shown in the thruster telemetry presented in the Appendix, the cathode-to-ground voltage was higher for the O condition as compared to all others, suggested worse cathode coupling. The role this has in reduced performance is unclear, as the M and M+O conditions had cathode-to-ground voltages comparable to other operating conditions.

Significant additional work is necessary with the thruster's magnetic field as the X3 continues through characterization. During this experiment, all six electromagnets were operated for all conditions, as it was found that the inner-channel magnets helped stabilize the cathode during middle- and outer-channel operation. However, the thruster was designed to operate each channel with only its two magnets; further work with magnetic field settings may allow for stable operation with only the magnets for the channels that are firing. The magnets of non-operating fields had an observable effect on plume structure, indicating that they likely affected performance as well. A similar effect was seen with the X2 NHT.[18]

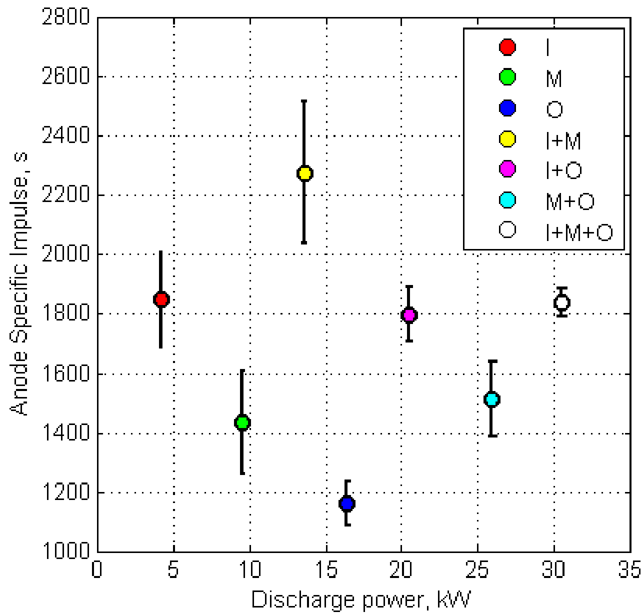


**Figure 5. Anode specific impulse versus discharge power across all operating conditions.**

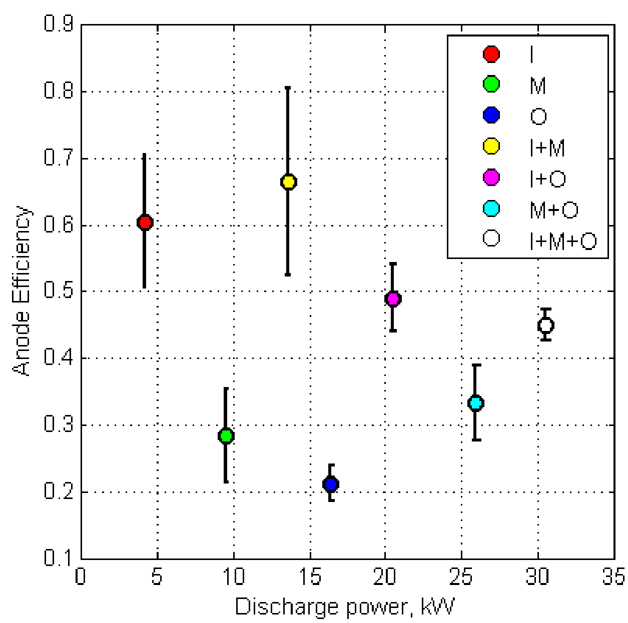


**Figure 6. Anode efficiency versus discharge power across all operating conditions.**

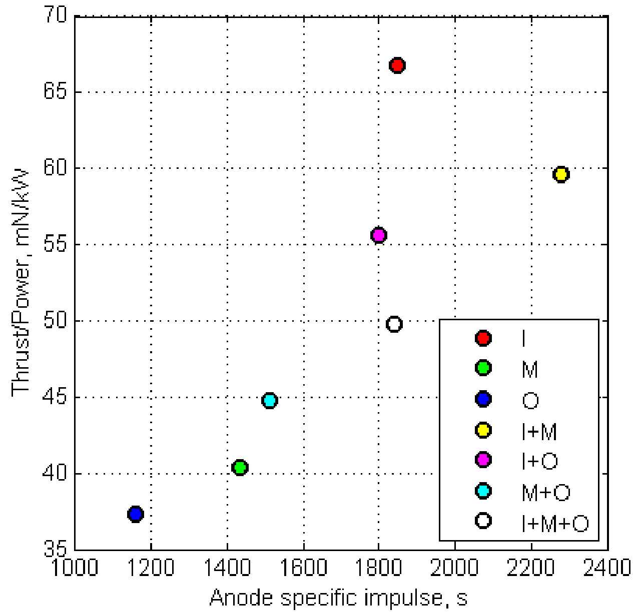


**Figure 7. Thrust-to-power ratio versus anode specific impulse.**

### B. Backpressure and Thruster Stability

As shown in Fig. 8, three of the operating conditions in this experiment fell significantly above the pressure cutoff (30 $\mu$Torr-Xe) for Hall thruster performance measurements as given in the standards guide.[13] No justification is given for this cutoff value, though throughout the literature reference is made to work by Randolph[19] in which the same cut-off of 30 $\mu$Torr-Xe is given for SPT-type thrusters. This value was based on a maximum for the amplitude of discharge current oscillations. Recent work suggests that changes in discharge current oscillations accompany changes in mode, and that these changes impact performance.[20,21] Those results indicate that the situation may not be as simple as the single-pressure threshold indicated by Randolph and by the standards guide.

In an effort to monitor thruster mode and stability, discharge current oscillations were monitored. The ratios of root-mean-square (RMS) discharge current oscillations ($I_{RMS}$) to the DC discharge current ($I_d$) for all firing conditions are presented in Table 2. Discharge current oscillation RMS values stayed below 38% of the mean discharge current across all operating conditions, and at times dropped below 10%. Amplitudes were smaller for the inner and middle channels in 2-channel operation than in 1- or 3-channel operation; the outer channel did not show such a clear trend. Analysis with a high-speed camera confirmed that all conditions were firmly in a breathing mode, not in a spoke mode.[22] However, the ratio of RMS current to mean discharge current did not remain constant for each channel across operating conditions. Analysis done by Dale[22] suggests that the strength of the breathing mode was also changing for each channel depending on firing configuration. It has been seen with multiple other Hall thrusters that changes in oscillations coincide with changes in performance,[20,21] and the X3 is expected to exhibit the same behavior.

This oscillation analysis indicates the higher chamber pressures experienced during some operating conditions did not induce major mode transitions (e.g. to a spoke mode or to a large-amplitude breathing mode) as compared to lower-pressure conditions. However, the variation in breathing strength likely coincides with variation in performance, something that will be studied in upcoming research. The mode transitions of the X3, and the roles that backpressure, magnetic field, and channel coupling play in these transitions, are not well understood yet.

As such, operation during this experiment did not appear to cross a pressure threshold, above which the thruster drastically changed mode, and the changes in breathing strength observed did not track with increasing pressure. A backpresure sweep (by elevating the chamber pressure through neutral xenon injector or throttling of chamber pumping speed) will help to confirm that the thruster performance is insensitive to

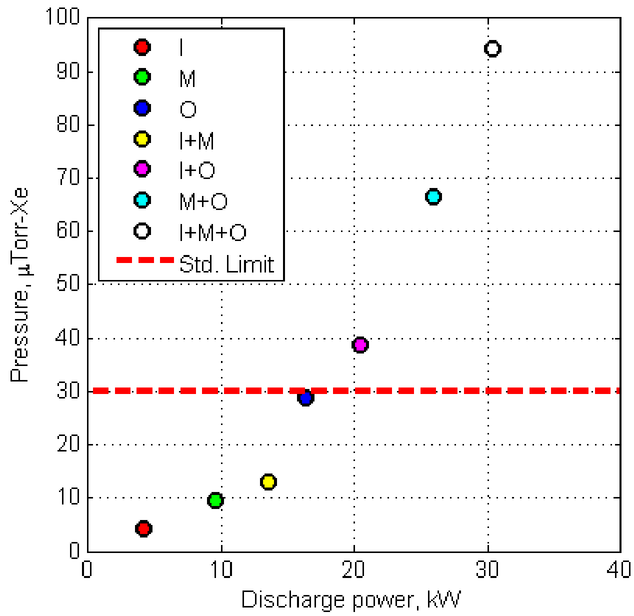


**Figure 8. The backpressure at each operating condition as compared to the maximum backpressure for Hall thruster performance measurements as stated in the industry standards guide.[13]**

**Table 2. The ratio of RMS discharge current oscillations to mean discharge current for each channel in all operating conditions.**

| Condition | $(I_{RMS}/I_d)_I$ | $(I_{RMS}/I_d)_M$ | $(I_{RMS}/I_d)_O$ |
|---|---|---|---|
| I | 0.23 | – | – |
| M | – | 0.24 | – |
| O | – | – | 0.32 |
| I+M | 0.12 | 0.04 | – |
| I+O | 0.09 | – | 0.32 |
| M+O | – | 0.16 | 0.37 |
| I+M+O | 0.29 | 0.21 | 0.28 |

backpressure at these levels, similar to the experiment done and the results found by Hofer with the H6MS.[16]

### C. Accounting for Backpressure Variations

Through holding the thruster at constant power, the difference in backpressure should not affect the thrust produced (ignoring the effects discussed above). However, it will affect both $I_{sp,a}$ and $\eta_a$, which are calculated using the anode mass flow rate (as discussed above, the anode mass flow rates are influenced by chamber backpressure during constant-power operation).

In an attempt to characterize this effect, the variation in each condition's total anode flow rates was compared to the summation of each channel running individually. As a maximum upper bound, the I+M+O condition is illustrated here. Because this condition saw the highest backpressure, the flow rates for each channel were the lowest compared to single-channel operation. In total, the I+M+O actual total anode flow rate was 15% lower than the sum of the I, M, and O anode flow rates.

Based on Eqs. 1 and 2, this 15% should translate to a 15% increase in both $\eta_a$ and $I_{sp,a}$ at the higher backpressure. This corresponds to increases of 0.07 and 250 s caused by backpressure effects on anode flow rates. The two-channel conditions, all at lower backpressure and thus lower flow rate variation, saw smaller increases than those for the I+M+O condition. These changes, though outside the error bars of most of the measurements, are not enough to affect the conclusions made above about performance of multi-channel operation compared to single-channel operation.

### D. Comparison to Other Thrusters

To better frame the relevance of these performance data, despite the significantly off-nominal current density, comparison was made to other state-of-the-art Hall thrusters at similar current densities. The thrusters chosen for this comparison were the NASA-300M,[23] NASA-400M,[24] NASA-457Mv1,[9] NASA-457Mv2,[25] and H6.[26]

The first of these comparisons is presented in Fig. 9. This indicates that the X3's operation falls along the same general thrust/discharge power line. This is to be expected because the X3's design is based heavily on these thrusters. It can be seen that the I+M condition, seen as high compared to the M and O conditions, actually falls closer to these other thrusters than the M or O conditions, suggesting that the M and O conditions are exhibiting poor performance, not that the I+M condition is exhibiting a "boost".

Additionally, the thrust-to-power ratio and anode efficiency are both plotted against anode specific impulse for the X3 and these other thrusters in Fig. 10. Both of these plots show that the X3's performance at particular operating conditions matches very closely with the performance of the other thrusters. Specifically, the I, I+O, and I+M+O operating conditions all cluster by the data from the H6 and the NASA Hall thrusters. This shows that, when operating at around 2000 s anode specific impulse, the thrust-to-power ratio of X3 is comparable to these thrusters. It can be seen in Fig. 10a that the low T/P commented on above for the M, O, and M+O conditions is off-nominal in both anode specific impulse and thrust-to-power ratio; further experiments are necessary to characterize the reasons for this.

### E. Uncertainty Analysis

The uncertainty for each thrust measurement was calculated by propagating the uncertainty in the measurement itself, in the calibration, and in the calibration parameters. Equations 3 through 7 detail the uncertainty for each thrust measurement:

$$T = a_2 \cdot V_{PID} + b_2 \tag{3}$$

$$T_{upper} = (a_3 + \Delta a_3) \cdot (V_{PID} + \Delta V_{PID}) + (b_3 + \Delta b_3) \tag{4}$$

$$T_{lower} = (a_1 - \Delta a_1) \cdot (V_{PID} - \Delta V_{PID}) + (b_1 - Deltab_1) \tag{5}$$

$$\Delta T_{upper} = T_{upper} - T \tag{6}$$

$$\Delta T_{lower} = T - T_{lower} \tag{7}$$

where $T$ is the thrust, $V_{PID}$ is the voltage required from the PID to keep the thrust stand in null mode, $a_{1,2,3}$ is the slope of the linear fit, $b_{1,2,3}$ is the intercept of the linear fit, and $\Delta$ is the uncertainty in the measurement listed. After shutdown, multiple calibrations of the thrust stand were performed. All calibrations were

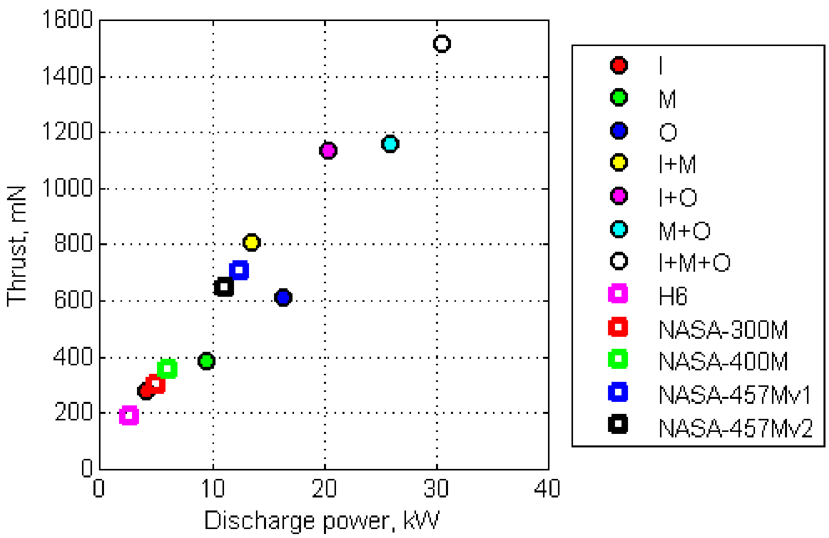


**Figure 9. A comparison of measured thrust to discharge power between the X3 and previous data from other state-of-the-art Hall thrusters at similarly low current densities.**

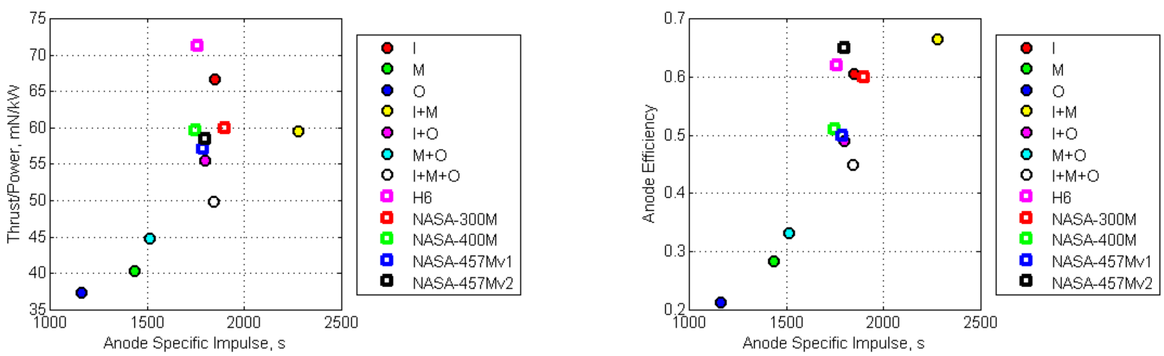


(a) T/P vs. $I_{sp,a}$

(b) $\eta_a$ vs. $I_{sp,a}$

**Figure 10. Performance metrics of the X3 compared to other state-of-the-art Hall thrusters at similarly low current densities.**

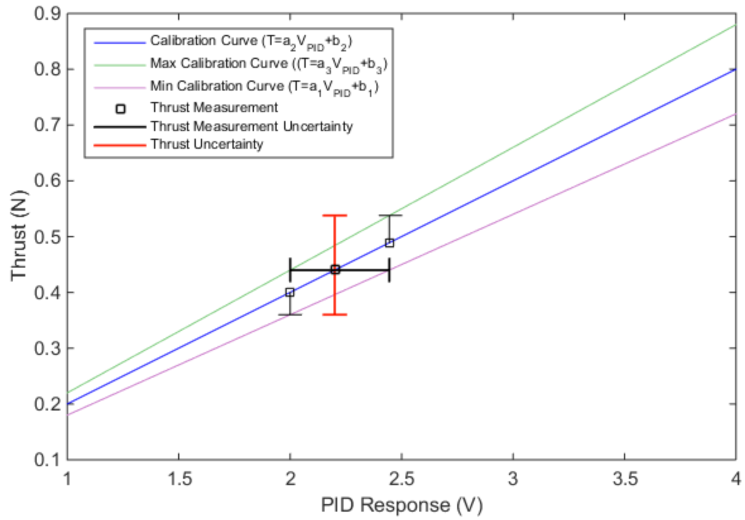


**Figure 11. An example plot of the thrust stand calibration curves, a thrust measurement, and the associated uncertainty in the measurement.**

averaged together to generate the calibration curve seen in Fig. 11. The PID voltage response to keep the thrust stand in the null position for each known weight was taken as the average of ten data points when each weight was dropped. The uncertainty of this value was taken as one standard deviation. Because the uncertainty in each calibration weight value is not necessarily constant, the different calibration curves may diverge or converge, as seen in Fig. 11. Due to this, the upper and lower bounds of uncertainty for each measurement may differ. The minimum and maximum calibration curves seen in Fig. 11 were calculated from the standard deviation of the calibration values. All other possible curves are assumed to lay within these bounds.

The PID signal response (in volts) for the thrust measurement was taken as the average of the last ten data points prior to the beginning of thruster shutdown. The uncertainty in the measurement was taken as one standard deviation from this set of data. The uncertainty in the thrust measurement was then applied to the maximum/minimum calibration curves to calculate the possible uncertainty in the calculation. Finally, in order to obtain the calibration curves, a linear regression fit was performed. Inherently, there is an error associated with the fit parameters. The uncertainty in these parameters was taken as the standard error calculated by the fit algorithm and then applied to the maximum and minimum values of thrust to calculate the total uncertainty.

# IV. Conclusions

The performance of the X3 in constant-power operation at 75% of its nominal current density has been measured. This performance has in general matched what was expected based on work done with other state-of-the-art Hall thrusters, though low anode efficiencies and anode specific impulses were seen for the M, O, and M+O conditions. A maximum thrust of 1518 mN was reported for the I+M+O condition at 30 kW total discharge power, with an anode specific impulse of 1840 s and an anode efficiency of 45.0%.

Performance dropped with increasing channel size during single-channel operation. The inner channel operated alone at this current density at an efficiency of 60.5%, providing 278 mN of thrust and an anode specific impulse of 1850 s. However, performance degraded for the middle and outer channels operating alone (though thrust increased as expected). The outer operating alone provided the worst performance of any operating condition in this experiment with an anode efficiency of 21.2% and a specific impulse of 1160 s. Reasons for this low performance are unclear.

Comparing performance to other state-of-the-art Hall thrusters showed that the performance of the I, I+O, and I+M+O conditions most closely match that of these other thrusters, with the M, O, and M+O conditions under-performing them and the I+M condition performing at higher anode efficiency and anode specific impulse.

# V. Future Work

To date, the X3 has been run up to 150% of its nominal current density and a total discharge power of 61 kW.[8] Thrust measurements have been obtained for discharge powers up to 30 kW. Moving forward, full performance and plasma plume characterization (using both time-averaged and time-resolved diagnostics) will proceed for the full thruster operating envelope, up to 200 kW discharge power. From there, magnetic field mapping and a more detailed study of channel interaction will occur. Throughout all of this work, the mode transitions of the X3, their effect on performance, and the role that backpressure, magnetic field settings, and cathode coupling play in them, will be studied.

# Appendix

| Parameter | I | M | O | I+M | I+O | M+O | I+M+O |
|---|---|---|---|---|---|---|---|
| $V_{D,I}$ [V] | 300 | – | – | 300 | 299 | – | 300 |
| $V_{D,M}$ [V] | – | 300 | – | 301 | – | 298 | 300 |
| $V_{D,O}$ [V] | – | – | 300 | – | 298 | 299 | 300 |
| $I_{D,I}$ [A] | 13.6 | – | – | 13.3 | 13.5 | – | 13.7 |
| $I_{D,M}$ [A] | – | 31.8 | – | 31.9 | – | 31.7 | 32.6 |
| $I_{D,O}$ [A] | – | – | 54.7 | – | 54.9 | 55.2 | 55.2 |
| $I_{D,T}$ [A] | 13.6 | 31.8 | 54.7 | 45.2 | 68.4 | 86.9 | 101.5 |
| $P_{D,T}$ [kW] | 4.2 | 9.5 | 16.4 | 13.6 | 20.4 | 25.9 | 30.4 |
| $\dot{m}_I$ [mg/s] | 15.3 | – | – | 10.6 | 10.6 | – | 10.6 |
| $\dot{m}_M$ [mg/s] | – | 27.4 | – | 25.7 | – | 25.8 | 21.4 |
| $\dot{m}_O$ [mg/s] | – | – | 53.8 | – | 53.9 | 52.5 | 52.2 |
| $\dot{m}_T$ [mg/s] | 15.3 | 27.4 | 53.8 | 36.3 | 64.5 | 78.3 | 84.2 |
| $\dot{m}_c$ [mg/s] | 1.53 | 2.74 | 5.38 | 3.63 | 6.45 | 7.83 | 8.42 |
| $T$ [mN] | 278 | 385 | 611 | 809 | 1136 | 1162 | 1518 |
| $\Delta(T)$ [mN] | +24/-22 | ± 47 | ± 39 | +88/-82 | +57/-60 | +97/-98 | +40/-41 |
| $I_{sp,a}$ [s] | 1850 | 1430 | 1160 | 2280 | 1800 | 1510 | 1840 |
| $\eta_a$ | 0.605 | 0.284 | 0.212 | 0.665 | 0.490 | 0.332 | 0.450 |
| $V_{c-g}$ [V] | -12.80 | -11.55 | -16.74 | -13.00 | -13.20 | -12.54 | -6.837 |
| $p_b$ [$\mu$Torr-Xe] | 4.4 | 9.6 | 29 | 13 | 39 | 66 | 94 |

# Acknowledgments

S. Hall is funded by a NASA Space Technology Research Fellowship under grant NNX14AL67H and the guidance of mentor Dr. Hani Kamhawi of NASA Glenn Research Center. A portion of this work was funded by the Air Force Office of Scientific Research through the Michigan/Air Force Center for Excellence in Electric Propulsion, and as such, the authors are thankful to Dr. Mitat Birkan and Dr. Daniel Brown for their generous support. The authors are thankful to Dr. Richard Hofer of JPL and Dr. Kunning Xu of the University of Alabama in Huntsville for their advice during the early stages of this experiment. Finally, special thanks to Dr. Dan Goebel at JPL for supplying the cathode for this experiment, along with exceptional operational guidance.

# References

[1]Brown, D. L., Beal, B. E., and Haas, J. M., "Air Force Research Laboratory High Power Electric Propulsion Technology Development," *2010 IEEE Aerospace Conference*, Big Sky, MT, March 2010.

[2]NASA, "Next Space Technologies for Exploration Partnerships Broad Agency Announcement," Oct. 2014.

[3]NASA, "Human Space Exploration Framework Summary," Jan. 2010.

[4]Liang, R. and Gallimore, A. D., "Constant-Power Performance and Plume Measurements of a Nested-Channel Hall-Effect Thruster," *32nd International Electric Propulsion Conference*, Wiesbaden, Germany, Sept. 2011.

[5]Liang, R. and Gallimore, A. D., "Far-Field Plume Measurements of a Nested-Channel Hall-Effect Thruster," *49th AIAA Aerospace Sciences Meeting*, American Institute of Aeronautics and Astronautics, Orlando, FL, Jan. 2011.

[6]Florenz, R. E., Gallimore, A. D., and Peterson, P., "Developmental Status of a 100-kW Class Laboratory Nested Channel Hall Thruster," *32nd International Electric Propulsion Conference*, Wiesbaden, Germany, Sept. 2011.

[7]Florenz, R. E., Hall, S. J., Gallimore, A. D., Kamhawi, H., Griffiths, C. M., Brown, D. L., Hofer, R. R., and Polk, J. E., "First Firing of a 100-kW Nested-channel Hall Thruster," *33rd International Electric Propulsion Conference*, Washington D.C., Oct. 2013.

[8]Hall, S. J., Florenz, R. E., Gallimore, A. D., Kamhawi, H., Brown, D. L., Polk, J. E., Goebel, D., and Hofer, R. R., "Implementation and Initial Validation of a 100-kW Class Nested-channel Hall Thruster," *50th AIAA Joint Propulsion Conference*, American Institute of Aeronautics and Astronautics, Cleveland, OH, July 2014.

[9]Manzella, D., Jankovsky, R., and Hofer, R., "Laboratory Model 50 kW Hall Thruster," *38th AIAA Joint Propulsion Conference*, American Institute of Aeronautics and Astronautics, Indianapolis, IN, July 2002.

[10]Beal, B. E., *Clustering of Hall effect thrusters for high-power electric propulsion applications*, Ph.D. thesis, University of Michigan, 2004.

[11]Goebel, D. M. and Chu, E., "High-Current Lanthanum Hexaboride Hollow Cathode for High-Power Hall Thrusters," *Journal of Propulsion and Power*, Vol. 30, No. 1, 2014, pp. 35–40.

[12]Chu, E., Goebel, D. M., and Wirz, R. E., "Reduction of Energetic Ion Production in Hollow Cathodes by External Gas Injection," *Journal of Propulsion and Power*, Vol. 29, No. 5, 2013, pp. 1155–1163.

[13]Dankanich, J. W., Walker, M., Swiatek, M. W., and Yim, J. T., "Recommended Practice for Pressure Measurements and Calculation of Effective Pumping Speeds during Electric Propulsion Testing," *33rd International Electric Propulsion Conference*, Washington D.C., 2013.

[14]Xu, K. G. and Walker, M. L., "High-power, null-type, inverted pendulum thrust stand," *Review of Scientific Instruments*, Vol. 80, No. 5, 2009, pp. 055103.

[15]Polk, J. E., Pancotti, A., Haag, T., King, S., Walker, M., Blakely, J., and Ziemer, J., "Recommended Practices in Thrust Measurements," *33rd International Electric Propulsion Conference*, Washington D.C., 2013.

[16]Hofer, R. R. and Anderson, J. R., "Finite Pressure Effects in Magnetically Shielded Hall thrusters," *50th AIAA/ASME/SAE/ASEE Joint Propulsion Conference*, AIAA, Cleveland, OH, 2014.

[17]Florenz, R. E., *The X3 100-kW Class Nested-Channel Hall Thruster: Motivation, Implementation, and Initial Performance*, Ph.D. thesis, University of Michigan, Ann Arbor, MI, 2013.

[18]Liang, R., *The Combination of Two Concentric Discharge Channels into a Nested Hall-Effect Thruster*, Ph.D. thesis, University of Michigan, Ann Arbor, MI, 2013.

[19]Randolph, T., Kim, V., Kaufman, H., Kozubsky, K., Zhurin, V. V., and Day, M., "Facility Effects on Stationary Plasma Thruster Testing," *23rd International Electric Propulsion Conference*, 1993, pp. 13–16.

[20]Sekerak, M. J., Longmier, B. W., Gallimore, A. D., Brown, D. L., Hofer, R. R., and Polk, J. E., "Mode Transitions in Hall Effect Thrusters," *49th AIAA/ASME/SAE/ASEE Joint Propulsion Conference*, 2013.

[21]Sekerak, M. J., Longmier, B. W., Gallimore, A. D., Huang, W., Kamhawi, H., Hofer, R. R., Jorns, B. A., and Polk, J. E., "Mode Transitions in Magnetically Shielded Hall Effect Thrusters," *50th AIAA/ASME/SAE/ASEE Joint Propulsion Conference*, American Institute of Aeronautics and Astronautics, Cleveland, OH, July 2014.

[22]Dale, E. T., Gallimore, A. D., and Huang, W., "High-Speed Image Analysis and Filtered Imaging of Nested Hall Effect Thruster Oscillations," *34th International Electric Propulsion Conference*, Hyogo-Kobe, Japan, July 2015.

[23]Kamhawi, H., Haag, T. W., Jacobson, D. T., and Manzella, D. H., "Performance Evaluation of the NASA-300M 20 kW Hall Effect Thruster," *47th AIAA Joint Propulsion Conference*, American Institute of Aeronautics and Astronautics, San Diego, CA, Aug. 2011.

[24]Peterson, P. Y., Jacobson, D. T., Manzella, D. H., and John, J. W., "The performance and wear characterization of a high-power high-Isp NASA Hall thruster," *41st Joint Propulsion Conference*, American Institute of Aeronautics and Astronautics, 2005.

[25]Soulas, G., Haag, T., Herman, D., and Huang, W., "Performance Test Results of the NASA-457M v2 Hall Thruster," *48th AIAA Joint Propulsion Conference*, American Institute of Aeronautics and Astronautics, Atlanta, GA, Aug. 2012.

[26]Brown, D. L., *Investigation of Low Discharge Voltage Hall Thruster Characteristics and Evaluation of Loss Mechanisms*, Ph.D. thesis, University of Michigan, Ann Arbor, MI, 2009.